Science and Technology Indonesia
e-ISSN:2580-4391 p-ISSN:2580-4405
Vol. 11, No. 3, July 2026

Research Paper

Interlinkage of Drought, Fire Severity, Vegetation Degradation, and Hydrological Response in Peatland Ecosystems

Mokhamad Yusup Nur Khakim[1,2*], Azhar Kholiq Affandi[1,2], Erni[1], Mardia Ulfa[2]

[1]Physics Department, Mathematics and Natural Science Faculty, Universitas Sriwijaya, Inderalaya, Ogan Ilir, South Sumatra, 30662, Indonesia
[2]Physics Graduate Program, Mathematics and Natural Science Faculty, Universitas Sriwijaya, Palembang, South Sumatra, 30139, Indonesia
*Corresponding author: myusup_nkh@mipa.unsri.ac.id

Abstract
Peatlands, as fragile ecosystems, are vulnerable to deforestation and altered hydrological regimes. The objectives of this study were to evaluate the effects of deforestation on runoff, drought, and fire severity in nine Peat Hydrological Units (KHG) in South Sumatra, Indonesia, in 2014–2025. The deforestation map was created by analyzing the Landsat-8 image through Spectral Mixture Analysis (SMA) and the Normalized Difference Fraction Index (NDFI). The runoff was modeled using the Soil Conservation Service-Curve Number (SCS-CN) method based on downscaled land cover, CHIRPS, GLDAS, and MODIS data. The drought condition was evaluated using the Vegetation Health Index (VHI), and fire severity was evaluated based on the Relativized Burn Ratio (RBR). The findings indicate that in 2015, the most significant deforestation occurred with the value of NDFI decreasing by > 0.25. In 2015, the highest annual rainfall during the study was 1828 mm, with an anomaly of 1-m topsoil moisture reaching -11.35 mm. Extreme drought (VHI < 0.1) occurred in $> 35\%$ of the area of S. Merang – S. Ngirawan and S. Lalan – S. Merang watersheds. Also, the 2015 fires had the largest area of moderate and high (RBR > 0.27) compared to the 2019 and 2023 fires. Deforestation also increased hydrologic response in the watershed as the annual runoff coefficient increased from 13% in 2015 to 15% in 2016 due to a decrease in infiltration from vegetation loss. As a conclusion, this study showed that deforestation increased runoff, drought conditions and peat fires. Our findings are important for evidence-based strategies on fire mitigation and hydrological management in tropical peatlands.

Keywords
Deforestation, Runoff, Drought, Fire Severity, Peatland Ecosystem

Received: 16 March 2026, Accepted: 29 May 2026
https://doi.org/10.26554/sti.2026.11.3.1106-1126

1. INTRODUCTION

Peatland plays an important role in maintaining biodiversity, water retention, and carbon sink capacity and therefore is essential in the efforts to prevent climate change (Pertiwi et al., 2021; Yule, 2010). However, peatlands are constantly threatened by deforestation and natural/human-induced degradation (Mishra and Singh, 2003; Szumińska et al., 2023). Deforestation has a direct effect on the water cycle in the sense that there is an increase of surface flow and a reduction of rain water absorption (Bruijnzeel, 2004; Hou et al., 2023; Ma et al., 2024; Peña-Arancibia et al., 2019; Potić et al., 2022). Further, it is well documented that carbon-rich peatland ecosystem are highly prone to land fires, particularly in dry season, especially when combined with deforestation (Datta and Krishnamoorti, 2022; Kiely et al., 2021; Nikonovas et al., 2020; Page et al., 2002). Several KHGs in Musi Banyuasin and western Banyuasin districts are designated as priority areas for management due to their high susceptibility to land fires and peatland degradation (Figure 1). These areas, which contribute to Indonesia's tropical peatland ecosystem, are exposed to vulnerability to land-cover change and hydrological disturbances; thus, studying deforestation dynamic, runoff, drought, and fires in the KHG spatial-temporally is necessary to support data-driven management.

The problem of deforestation still needs to be seriously attended and managed today. In Brazil the deforestation rates in Mato Grosso were calculated with SMA methods which showed a decrease in rates of 28.8% between 1986 and 2020 (Halbgewachs et al., 2022). This technique has been proven to be effective in detecting forest degradation in Paragominas, Pará, Brazil, in the form of logging and burning between 2000 and 2015 (Hasan et al., 2019). However, in these studies, the application of the SMA method has been limited to specific situations and types of the areas, which restricts their use for tropical peat forest areas.

The Soil Conservation Service-Curve Number (SCS-CN)

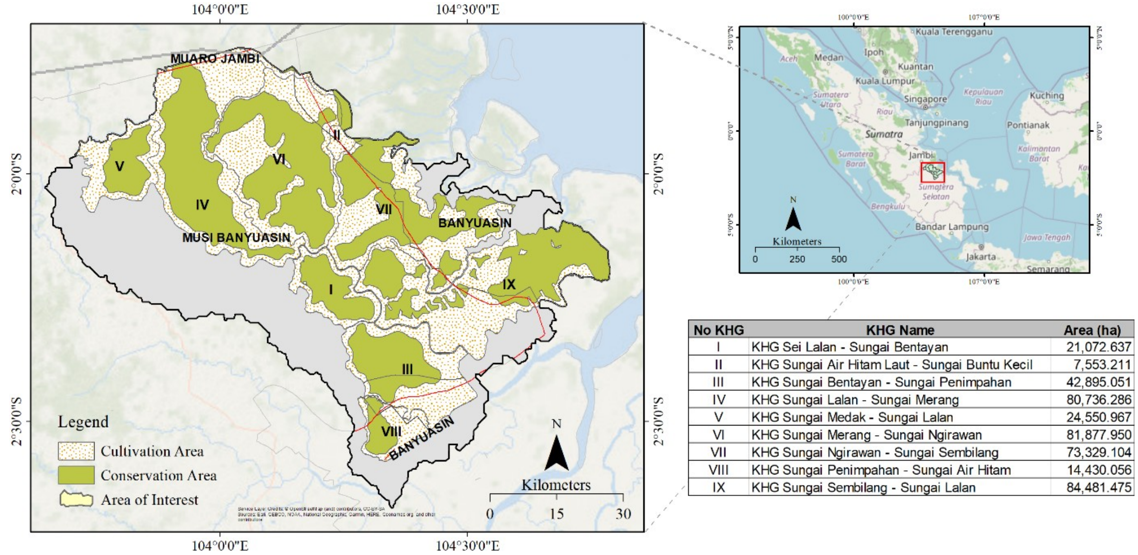

No KHG	KHG Name	Area (ha)
I	KHG Sei Lalan - Sungai Bentayan	21,072.637
II	KHG Sungai Air Hitam Laut - Sungai Buntu Kecil	7,553.211
III	KHG Sungai Bentayan - Sungai Penimpahan	42,895.051
IV	KHG Sungai Lalan - Sungai Merang	80,736.286
V	KHG Sungai Medak - Sungai Lalan	24,550.967
VI	KHG Sungai Merang - Sungai Ngirawan	81,877.950
VII	KHG Sungai Ngirawan - Sungai Sembilang	73,329.104
VIII	KHG Sungai Penimpahan - Sungai Air Hitam	14,430.056
IX	KHG Sungai Sembilang - Sungai Lalan	84,481.475

Figure 1. Spatial Distribution and Areal Statistics of Peatland Hydrological Units (KHGs) within the Study Area

method is well known as runoff modeling. Studies on SCS-CN have described its development, implementation, and basis theory (Mishra et al., 2021). The precision of the SCS-CN procedure can be improved as some inconsistencies and other problems Michel et al. (2005) are present. The relationship between the curve number and the initial abstraction has been evaluated by some researchers in recent studies trying to find a way of improving the accuracy of SCS-CN model prediction Brandão et al. (2025) which needs further testing under different climatic and hydrological conditions.

In the case of remote sensing technology, the Vegetation Health Index (VHI) measures drought conditions by considering the Vegetation Condition Index (VCI) and the Temperature Condition Index (TCI). It can be used in different environments as it considers local biochemical and climatic conditions (Zeng et al., 2023). Improved accuracy was observed where the weighting of VCI and TCI is adjusted depending on the regional climatic conditions and type of vegetation. The combination of VHI and normalized difference vegetation index (NDVI) has been found to be a good approach in drought assessment in Niamey in southwestern Niger (Almouctar et al., 2024)). However, the study has its limitations because of specific study areas that limit their generalizability of the results.

The two most widely utilized fire severity indicators based on Landsat data are the normalized burn ratio (NBR) and relative burn ratio (RBR) (Miller and Thode, 2007; Soverel et al., 2010), both of which derive from normalized burn ratio. Relative burn ratio is a proxy of both metrics and demonstrates better overall classification accuracy to distinguish severity classes (Parks et al., 2014). Relative burn ratio has been used to explore variability and drivers of fire severity in northwestern Canadian boreal forests (Whitman et al., 2018), but results do not offer specific, practical guidance for application in the field. When relative burn ratio is integrated with machine learning it is more accurate at classifying fire severity maps in the Italian Western Alps (Morresi et al., 2022).

Most previous studies have analyzed only a portion of the processes examined here. Analyses of spectrally un-mixed area fractions have been common to map the distribution of deforestation and degraded forest, especially across the Brazilian Amazon and other tropical forests, but NDFI alterations are rarely examined in tandem with downstream hydrological responses or fire (Bullock et al., 2020; Halbgewachs et al., 2022; Hasan et al., 2019; Souza et al., 2005, 2013). Similarly, vegetation health index has been used to examine drought at regional to global scales but usually focuses on vegetation conditions and does not directly examine drought anomalies in conjunction with fire or runoff (Almouctar et al., 2024; Burka et al., 2024; Zeng et al., 2022, 2023). Relative burn ratio and other related burn-severity indices have been used to characterize fire in boreal and temperate forests but rarely in conjunction with multi-year deforestation trends or hydrological variables in tropical peatlands (Miller and Thode, 2007; Morresi et al., 2022; Parks et al., 2014; Soverel et al., 2010; Whitman et al., 2018).

Furthermore, studies using the Soil Conservation Service curve number (SCS-CN) generally examine land-use and land-cover change and runoff within a specific area and seldom couple estimates of runoff with VHI and RBR in peat environments (Michel et al., 2005; Mishra and Singh, 2003; Singh et al., 2023). Recent studies conducted at the regional scale have also recognized the role of hydroclimatic variation within peatland and fire prone landscapes of Sumatra: diurnal rainfall regime characteristics in the peatland areas in South Sumatra can have direct impacts on local water conditions, and high variation in rainfall across the eastern coast of Sumatra are associated with forest and land fires occurring under extreme climate phenomena including ENSO and Indian Ocean Dipole

(Mandailing et al., 2020; Suhadi et al., 2023).

This study analyzed the combined impact of deforestation and climate using four indicators over a 12-year period (2014-2025) for nine peat hydrological units in South Sumatra: normalized difference forest index (NDFI) derived from spectrally un-mixed area fractions (SMA), runoff coefficients from SCS-CN based curve number, drought intensity classes from vegetation health index (VHI), and fire severity classes from relative burn ratio (RBR). We thereby produce a temporally consistent set of annual maps and timeseries describing deforestation, runoff, drought and fire severity for the entire region. These can now be compared and correlated to assess how these factors are related to each other in time and space. To our knowledge, no previous study has analyzed these four components together over the same temporal extent (a decade of annual data) and spatial extent in the tropical peatlands of Sumatra and none have quantitatively assessed how these indicators are linked to each other in terms of deforestation, runoff coefficient, drought intensity and fire severity at this scale.

2. EXPERIMENTAL SECTION

2.1 Materials

This study used several datasets of satellite remote sensing data and environmental factors to assess the patterns of deforestation, hydrological responses, drought variations, and fire intensity in tropical peatland ecosystems. Most of the data processing and analysis were performed using Google Earth Engine (GEE), a cloud-based geospatial platform. This made it possible to process large volumes of satellite data and to analyze changes over time.

The main data used to map deforestation and forest degradation were optical images acquired by Landsat-8. Landsat-8 provides surface reflectance data in the visible, near-infrared and shortwave infrared spectral bands. This information is needed to calculate vegetation indices and estimate fire intensity.

Moderate-resolution imagery from the Moderate Resolution Imaging Spectroradiometer (MODIS) was used to support land-cover characterization and drought monitoring. MODIS land cover products were used as the baseline information for land surface classification, and MODIS-derived Normalized Difference Vegetation Index (NDVI) and Land Surface Temperature (LST) were used to assess vegetation health and thermal stress related to drought conditions.

Sentinel-1 radar data were used as additional predictor variables. Synthetic Aperture Radar (SAR) imagery provides information about the structure of vegetation and the condition of the land surface. This is especially useful in tropical areas, where constant cloud cover often makes optical observations difficult.

Rainfall data were sourced from the Climate Hazards Center InfraRed Precipitation with Station data (CHIRPS), a dataset offering extended precipitation observations, thereby facilitating analyses of hydrological and climate variability. Soil properties were determined by USDA Soil Texture Classification and runoff modeling and hydrological analysis were performed.

To assess climate anomalies affecting drought and fire dynamics, soil moisture and soil temperature data were acquired from the Global Land Data Assimilation System (GLDAS). Moreover, the Global Human Settlement Layer (GHSL) served as supplementary data to enhance land-cover classification and pinpoint regions impacted by human activities.

2.2 Methods

Cloud-based geospatial analysis platform Google Earth Engine was used for most of the pre-processing of satellite data, data compositing, and spatial analysis. Google Earth Engine provides easy access to large archives of satellite and other Earth observation data, and allows to parallelize processing of multiple satellite images in the cloud.

In the GEE environment, several satellite datasets such as Landsat-8, MODIS, Sentinel-1, CHIRPS (Climate Hazards Group InfraRed Precipitation with Station data), and GLDAS (Global Land Data Assimilation System) datasets were utilized and processed in order to derive spatial indicators such as deforestation, hydrological response, drought, and fire severity. The main steps of the methodology are depicted in Figure 2.

2.2.1 Deforestation Mapping

Deforestation and forest degradation were monitored using time-series analysis of Landsat-8 data. Selective logging can be challenging to detect as it often involves sub-pixel canopy damage. In order to overcome this problem, the Spectral Mixture Analysis (SMA) technique was applied to model sub-pixel composition of the pixels. Spectral mixture analysis (SMA) is employed to unmix mixed pixels into fractions of different land cover types (Bullock et al., 2020). The method employs a linear spectral unmixing model to determine the fractional amounts of different endmembers. The generalized extended Spectral Mixture Analysis (SMA) model described by Souza et al. (2005), comprises five end-members commonly found in degraded tropical forests: Green Vegetation (GV), Non-Photosynthetic Vegetation (NPV), Soil, Shadow, and Cloud. In this study, candidate endmembers were extracted from spectrally pure pixels identified in Landsat-8 surface reflectance images through visual inspection of RGB composites (e.g., bands 4-3-2 and 5-4-3) and examination of spectral profiles. Pixels representing dense, intact forest canopies were used for the Green Vegetation (GV) endmember, while senescent or dry vegetation and logging residues were used for the Non-Photosynthetic Vegetation (NPV) endmember. Exposed mineral surfaces were selected for the Soil endmember, deep canopy and terrain shadows were used for the Shadow endmember, and optically thick clouds were chosen for the Cloud endmember. The resulting spectral signatures were compared with typical tropical forest spectra reported in previous SMA applications to ensure their physical plausibility.

The adequacy of the selected endmembers was evaluated by analysing the resulting fraction images and NDFI maps. Frac-

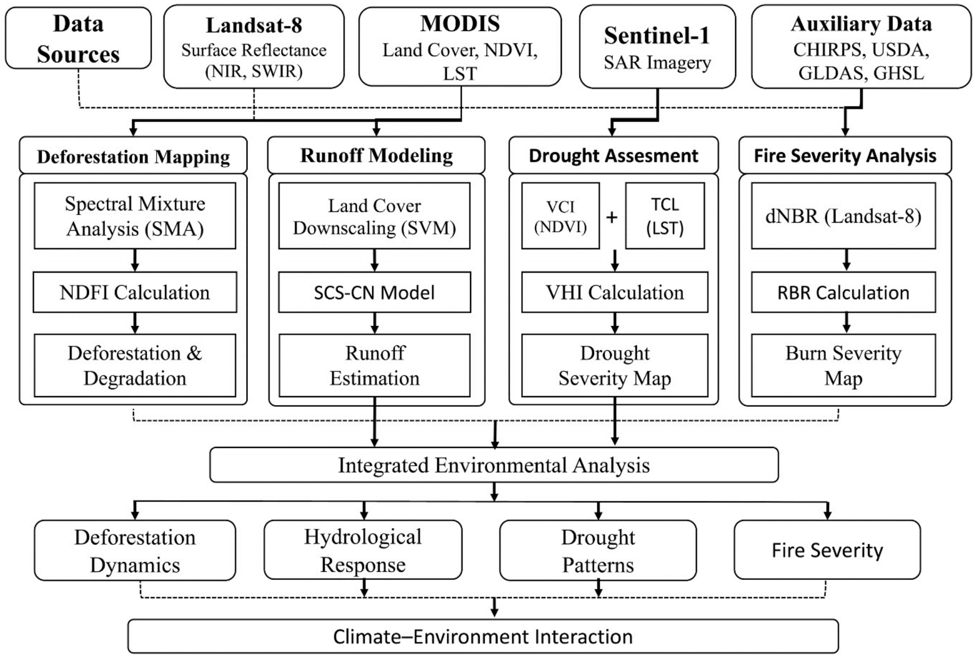

Figure 2. Methodological Workflow of the Integrated Environmental Analysis Using Multi-Source Remote Sensing Data

tional abundances were checked to remain within the range and to sum close to 1 for most pixels, and intact forest areas exhibited high GVshade fractions and low NPV and Soil fractions, whereas logged or degraded forests showed reduced GV and increased NPV and Soil, consistent with Souza et al. (2005, 2013). In addition, fraction and NDFI maps were visually compared with known logged or burned areas and high-resolution imagery within the peat hydrological units to verify that spatial patterns of degradation were realistically captured.

Based on the resulting fraction images, the Normalized Difference Fraction Index (NDFI) was computed, which is used to detect forest disturbance: where, GVshade, NPV, and Soil are the proportions of the Green Vegetation in shadow, NPV, and Soil end-members, respectively. NDFI ranges from -1 (when the GVshade fraction approaches 0) to 1 (when NPV and Soil fractions approach 0). The NDFI values for intact forests are usually high, which are characterized by high GVshade fractions and low NPV and Soil fractions. Logged or degraded forests usually present lower GV and Shadow fractions, and higher NPV and Soil fractions. The changes in NDFI between the two consecutive years of observations were used to identify deforestation and forest degradation.

2.2.2 Runoff Modeling

Surface runoff was determined with the soil conservation service curve number (SCS-CN) method (Mishra and Singh, 2003; Singh et al., 2023). No calibration was done since there were no observed discharge data in the ungaged catchments in the study area, but SCS-CN is appropriate for such conditions as it allows for an estimation of surface runoff on the basis of the physical parameters of the watersheds like soils and land uses instead of requiring a long stream flow record (Mishra and Singh, 2003; Soil Conservation Service, 1972; United States Department of Agriculture, N.R.C.S., 2004).

In the present study, the CN values and initial abstraction coefficient (λ) were selected by using the regional studies (standard procedure adopted from (SCS, 1986) tables and have been tested on the similar environmental set up. Thus, the use of standard values of CN and $\lambda = 0.2$ give a uniform and reasonable basis for spatial temporal runoff analysis in the study area (Mockus, 1949; Singh et al., 2023).

The SCS-CN method uses data on rainfall, land use and type of soil to estimate the volume of surface runoff. Rainfall data for this study were obtained from the Climate Hazards Group InfraRed Precipitation with Station (CHIRPS) data (Funk et al., 2015), while land use data were obtained from the MODIS land cover data (Friedl et al., 2010). Information on soil type was obtained from the United States Department of Agriculture (USDA) texture classes (Hengl, 2018). As the spatial resolution of MODIS land cover data is ~ 500 m, we applied a downscaling approach to obtain land cover at a finer resolution. A Support Vector Machine (SVM) machine learning method was used for the downscaling process (Cortes and Vapnik, 1995; Pisner and Schnyer, 2020). The support vector machine (SVM) classification model used several predictor variables. Landsat-8 surface reflectance data, Sentinel-1 backscatter data and other information from the Global Human Settlement Layer (GHSL) Pesaresi et al. (2024) were used as the data.

Other variables included NDVI and NDWI, and percentile composite of Landsat-8 spectral bands. Stratified sampling approach was used to collect training samples, and the SVM classifier was implemented to downscale the MODIS land cover map from 500 m to 50 m. Then, the downscaled land cover data was used for runoff estimation for each land cover type.

2.2.3 Drought

We calculated the Vegetation Condition Index (VCI) and Temperature Condition Index (TCI) based on MODIS NDVI and land surface temperature (LST) to determine the drought conditions for the study area. The VCI represents the drought condition of vegetation compared with the same period of the past highest and lowest value. The NDVI values for minimum and maximum from 2000 to analysis year were obtained for calculating VCI. TCI was calculated to calculate the drought conditions based on temperature. It shows how hot the temperature in a given time compared with historical values. The temperature conditions were derived using the MODIS LST product to determine TCI.

Vegetation Health Index (VHI) was calculated by combining VCI and TCI values (Burka et al., 2024; Zeng et al., 2022). VHI integrates the information of vegetation condition and thermal anomalies in the image for the more robust drought intensification representation. According to the severity, VHI was classified into five categories based on VHI values, which included extreme drought for VHI < 0.1, severe drought for VHI ≤ 0.2, moderate drought for VHI ≤ 0.3, mild drought for $0.3 \leq$ VHI < 0.4, and no drought for VHI > 0.4. These categories were selected to categorize the intensity of drought in the study area.

In this study, VHI values were used to categorize drought into five categories as extreme drought: VHI < 0.10, severe drought: VHI ≤ 0.20, moderate drought: VHI ≤ 0.30, mild drought: $0.30 \leq$ VHI < 0.40, and no drought: VHI > 0.40. This category of VHI was found in earlier applications based on VHI indices in which it is shown in the case of lower VHI values have a higher severity of stress on vegetation (Burka et al., 2024). In this study, the classification of different categories of VHI is based on different thresholds used in previous studies on VHI drought indices. The threshold value of VHI was also tested to categorize VHI values into the different severity of drought. In this experiment, the VHI was categorized into different categories by changing the threshold value of VHI as ± 0.05–0.10 and the results are not very different, which is found in previous studies on different categories of the drought condition from the VHI. The maps showed different areas in case of higher severity level of drought are same, and year with extreme drought conditions were found in 2015, similar to our result in this study, thus suggesting the robustness of our conclusions to alternative thresholds.

2.2.4 Fire Severity

The Differenced Normalized Burn Ratio (dNBR) maps are applied to determine the burned area, obtained by differencing the pre-and post-fire NBR values. The NBR is computed from the near infrared (NIR) and shortwave infrared (SWIR) Landsat band (Burka et al., 2024; Zeng et al., 2022). But it may not reflect the true fire severity based on the low vegetation density before fire. So the Relativized Burn Ratio (RBR) is used to show the relative change of burned area. RBR values were grouped into seven categories, namely: High Regrowth, Low Regrowth, Unburned, Low Severity, Moderate-Low Severity, Moderate-High Severity, and High Severity.

The study mainly focuses on the results of deforestation mapping, runoff, drought levels, and fire severity. The maps could also be validated with field observation. The relationship among natural factors that contribute to the dynamic of runoff, drought, and fire severity is investigated by analyzing their relationship with climatic anomalies. Climatic anomalies includes rain fall, soil moisture, and temperature. Rain fall dataset is obtained from CHIRPS while soil moisture and temperature datasets are obtained from the Global Land Data Assimilation System (GLDAS) (Rodell et al., 2004).

2.3 Validation Approach

The reliability of the derived indicators was assessed by combining several independent satellite-based datasets and existing land-cover products (Table 1). To prove the reliability of the NDFI map based on the SMA and its accuracy in representing deforestation and vegetation degradation, these maps were compared with MODIS land cover classes and the location of VIIRS hotspot clusters in the years where substantial forest cover was lost (i.e. 2015, 2019 and 2023). The regions that showed significant reduction in NDFI overlapped generally with the transition of MODIS pixels from forest to non-forest classes, in addition to the regions with a higher density of hotspot clusters, which confirms the consistency of the deforestation products. The results from the SVM based land cover downscaling (i.e. confusion matrix, accuracy overall and Kappa) confirm that the land cover used as input for the runoff modelling was reliable.

Furthermore, to confirm the accuracy of the classification based on VHI to represent the drought severity, we compared VHI based drought categories to CHIRPS rainfall anomalies and GLDAS soil moisture anomalies. Years where large areas of extreme and severe drought (i.e. VHI <0.2) were classified corresponded to those with rainfall and soil moisture anomalies below the mean especially in 2015, suggesting the VHI classification was consistent with independent hydrometeorological datasets.

For fire severity, we compared RBR maps to the density of VIIRS hotspots and the size of known fires. Moderate and high severity categories showed a spatial overlap with the areas where higher density of hotspot clusters is found and with the burned area, suggesting the spatial patterns of fire impact captured by RBR in the peat hydrological units are reliable.

3. RESULTS AND DISCUSSION

3.1 Analysis of Climate Conditions in the Study Area

Climate variability plays an important role in understanding the relationship between drought, land degradation, fire regime,

Table 1. Data Sources and Validation Approach

Indicator	Primary Data/Source	Derived Product	Validation / Consistency Check
Deforestation / vegetation degradation	Landsat-8 surface reflectance (SMA, NDFI)	Annual NDFI-based deforestation and degradation maps	Consistency with MODIS land-cover transitions (forest → non-forest) and high-density hotspots during major fire years (2015, 2019, 2023).
Land cover (for runoff)	MODIS land cover, Landsat-8, Sentinel-1, GHSL (SVM downscaling)	50 m land-cover map (SVM downscaling)	Confusion matrices, overall accuracy, and Kappa for SVM classification, indicating reliable land-cover inputs for runoff modelling.
Runoff	CHIRPS rainfall, SCS-CN with USDA soil texture and land cover	Annual runoff depth and runoff coefficient per KHG	Indirect consistency with changes in land cover and inter-annual variability in rainfall and water storage anomalies from GLDAS.
Drought	MODIS NDVI and LST (VHI)	VHI-based drought categories	Agreement between extreme/severe drought years (VHI < 0.2) and negative rainfall anomalies (CHIRPS) and soil moisture deficits (GLDAS), especially in 2015.
Fire severity	Landsat-based NBR/dNBR (RBR)	RBR-based fire severity classes	Spatial correspondence between moderate–high severity classes and high VIIRS hotspot densities and known large fire years (2015, 2019, 2023).

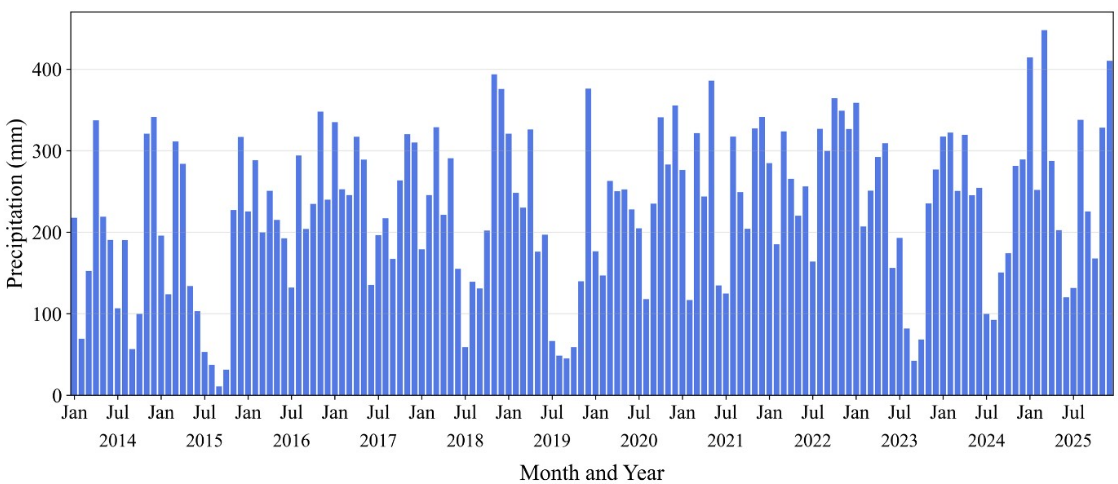

Figure 3. Temporal Variation of Monthly Rainfall Amount Over the 2014–2025 Period

and hydrological responses in peatlands. To examine the changes in climate conditions over the study area, we used monthly rainfall over the study area from Climate Hazards Center InfraRed Precipitation with Station data (CHIRPS). The monthly rainfall data shows multiple dry periods, indicating severe drought occurrence (Figure 3). The driest condition occurred in 2015, when there was very little rain from May to October. Similar conditions occurred in 2019 (drought from July to October) and 2023 (drought from August to October). Drought occurrence in these years is expected as a significant El Niño event occurred in those years, greatly reducing rainfall over Southeast Asia (Field et al., 2009; Huijnen et al., 2016). Annual rainfall over the study area confirms the observation. The lowest annual rainfall was in 2015 (1,828.34 mm) followed by

Table 2. Comparison of This Study with Selected Previous Studies on Deforestation, Drought, Fire Severity, and Runoff

Study / reference (example)	Region & ecosystem	Period	Main indicators / methods used	Processes analysed jointly	Key contributions / limitations relative to this study
Souza et al. (2005, 2013)	Brazilian Amazon, tropical forest	~1990s–2005	SMA and NDFI for logging and forest degradation	Deforestation / degradation only	High-resolution mapping of logging and degradation using SMA; no explicit analysis of runoff, drought, or fire severity; not focused on peat hydrological units.
(Zeng et al., 2022, 2023)	Global / various vegetation types	2001–2023	VHI and improved global VHI datasets for drought monitoring	Drought only	Advanced global VHI datasets; do not integrate fire severity or runoff, and are not specific to tropical peatlands.
Parks et al. (2014); Whitman et al. (2018)	North American boreal / temperate forests	Single events or multi-year fire records	NBR/dNBR and RBR for burn severity classification	Fire severity only	Detailed fire severity mapping; limited integration with deforestation trajectories, drought indices, or hydrological response; non-peat ecosystems.
Singh et al. (2023) and related SCS-CN applications	Various catchments (non-peat)	Single events or limited multi-year records	SCS-CN runoff modelling using land use and soil type	Runoff / hydrology applications	Evaluate runoff response to land-use change; do not combine with SMA-based deforestation, VHI, or RBR in peat hydrological units.
This study (South Sumatra peat hydrological units)	Nine tropical peat hydrological units, South Sumatra	2014–2025	SMA-derived NDFI, SCS-CN runoff, VHI drought, RBR fire severity	Deforestation, runoff, drought, fire severity jointly	Integrates four indicators over 12 years to quantify interlinkages between deforestation, runoff coefficients, drought intensity, and fire severity in tropical peat hydrological units; provides spatially explicit, multi-process assessment in a fire-prone peatland region.

2019 (2,233.39 mm) and 2023 (2,471.83 mm). The decline of annual rainfall was expected to influence the hydrological stability of peatland ecosystems as the peatland hydrological system was mainly controlled by shallow groundwater storage (Page et al., 2002; Turetsky et al., 2015). The results are consistent with recent regional studies in Sumatra, which have shown that large-scale climate variability, especially the ENSO and the Indian Ocean Dipole, strongly influence the extremes of rainfall and participate in the occurrence of forest and land fires in the region (Akhsan et al., 2023).

Variations of monthly rainfall influence the response of soil temperature and moisture. Soil temperature and moisture data were acquired from NASA Global Land Data Assimilation System Version 2 (GLDAS-2). Anomalies of soil temperature and moisture describe the deviation from the mean value for the study period (Figure 4). Soil moisture showed a significant decrease in severe drought years. The largest negative anomaly was recorded in October 2015 (-11.35 mm) , followed by September 2019 (-6.54 mm) and October 2023 (-5.44 mm) . Negative anomalies represented that the soil moisture was lower than the average condition, suggesting the peat surface layer was dry. Conversely, the anomalies of soil temperature showed a negative relationship with soil moisture anomalies. As the negative anomaly of soil moisture increased, the anomaly of soil temperature increased. The increase in soil temperature is attributed to peat drying and evapotranspiration, which is important for the peatland ecosystems as the moisture content of the uppermost peat layer plays a key role in peat fire frequency (Kettridge et al., 2015; Page et al., 2002).

3.2 Spatial-Temporal Variation of Drought Severity

To understand drought severity, we used the VHI time series data over the study region during 2014 to 2025. This multi-year study can help to identify the extreme years of droughts and to verify the drought conditions over the study region. A simple sensitivity test using slightly modified VHI thresholds (±0.05-0.10) produced similar spatial patterns of drought severity, and 2015 consistently emerged as the year with the

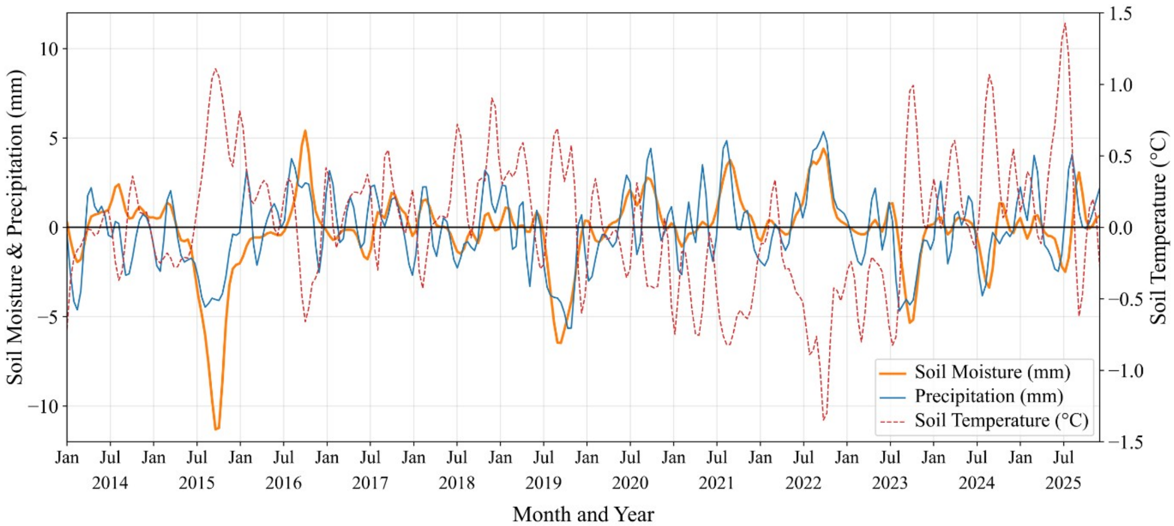

Figure 4. Monthly Anomalies of Precipitation, Soil Moisture, and Soil Temperature from 2014 to 2025

largest extent of extreme and severe drought, confirming that the key drought patterns are not strongly dependent on the exact threshold values. Figure 5 shows the spatial distribution of drought severity (VHI) across the peatlands of South Sumatra. The highest magnitude of drought occurred in 2015, as extensive areas with very low VHI values were observed, particularly over S. Merang - S. Ngirawan and S. Lalan - S. Merang peat hydrological units (KHG). The two peat KHGs are classified as conservation forests, yet, they experienced severe drought conditions over the study region.

Low VHI values show that the vegetation is under a high level of physiological stress due to the lack of water. Persistent droughts result in a reduction of the water table of the peatlands, which leads to the drying of the peat. Consequently, the dry peat is a highly flammable fuel, increasing the chances of ignition and spread of fires. The droughts were less intense in the following years and in 2019 and 2023 only some parts of the region experienced moderate to extreme drought.

In addition, the extent of the droughts in 2019 and 2023 was smaller than that of the 2015 extreme drought. In 2025, droughts were also limited to a few areas, mainly in S. Bentayan - Penimpahan KHG. Figure 6 shows the temporal variations of extreme droughts over the study area. The most severe drought was observed in 2015, succeeded by a decline that persisted until 2017, and subsequently, an escalation in 2019, which then diminished progressively until 2025, notwithstanding a minor rise in 2023 and 2024. Whereas, 2022 and 2025 represented non-drought conditions accounting for about 90% and 93.9% of the study area, respectively. This highlights the importance of inter-annual climate variability on the drought dynamics of the study region. Furthermore, years with widespread extreme and severe drought (VHI <0.2) are associated with negative anomalies of rainfall and soil moisture derived from CHIRPS and GLDAS, especially in 2015, confirming the consistency of VHI-based drought classification with independent hydrometeorological datasets.

3.3 Fire Occurrence and Severity Patterns

Fire occurrence over the study region was first identified from the VIIRS hotspots data. Hotspots are thermal anomalies that correspond to actively burning fires, either on the surface or within the peat layers. Figure 7 shows the spatial distribution of hotspots over the study region. It can be seen that the highest fire activity occurred in 2015. However, the number of hotspots detected in 2019 was relatively low and mainly concentrated over S. Lalan – S. Merang peat hydrological unit. The spatial distribution of hotspots clearly matched the areas affected by drought. The evidence suggests that the severe drought conditions were a key factor in the occurrence of peatland fires.

To assess the ecological impacts of those fires, we evaluated the fire severity using the Relative Burn Ratio (RBR). Figure 8 shows the fire severity map derived from the RBR approach. The spatial patterns of fire severity map are consistent with the drought severity and hotspot distribution maps, particularly during the extreme fire event in 2015. However, the hotspot distribution and fire severity map show a relatively poor agreement in 2023 and 2025. The mismatch is partly related to the spatial resolution of the VIIRS data (nominal pixel size ~375 m, equivalent to ~14 ha per pixel), which limits its ability to detect low-intensity fires or small burned patches below this scale. As a result, some moderate to high severity burns captured by the higher-resolution Landsat-based RBR may not be associated with any detected VIIRS hotspot, particularly when the burned area is smaller than a single VIIRS pixel or partially obscured by cloud and smoke. This scale effect can lead to an underestimation of hotspot counts in areas where RBR still indicates substantial fire impact and should be considered when interpreting the relationship between hotspot density and fire

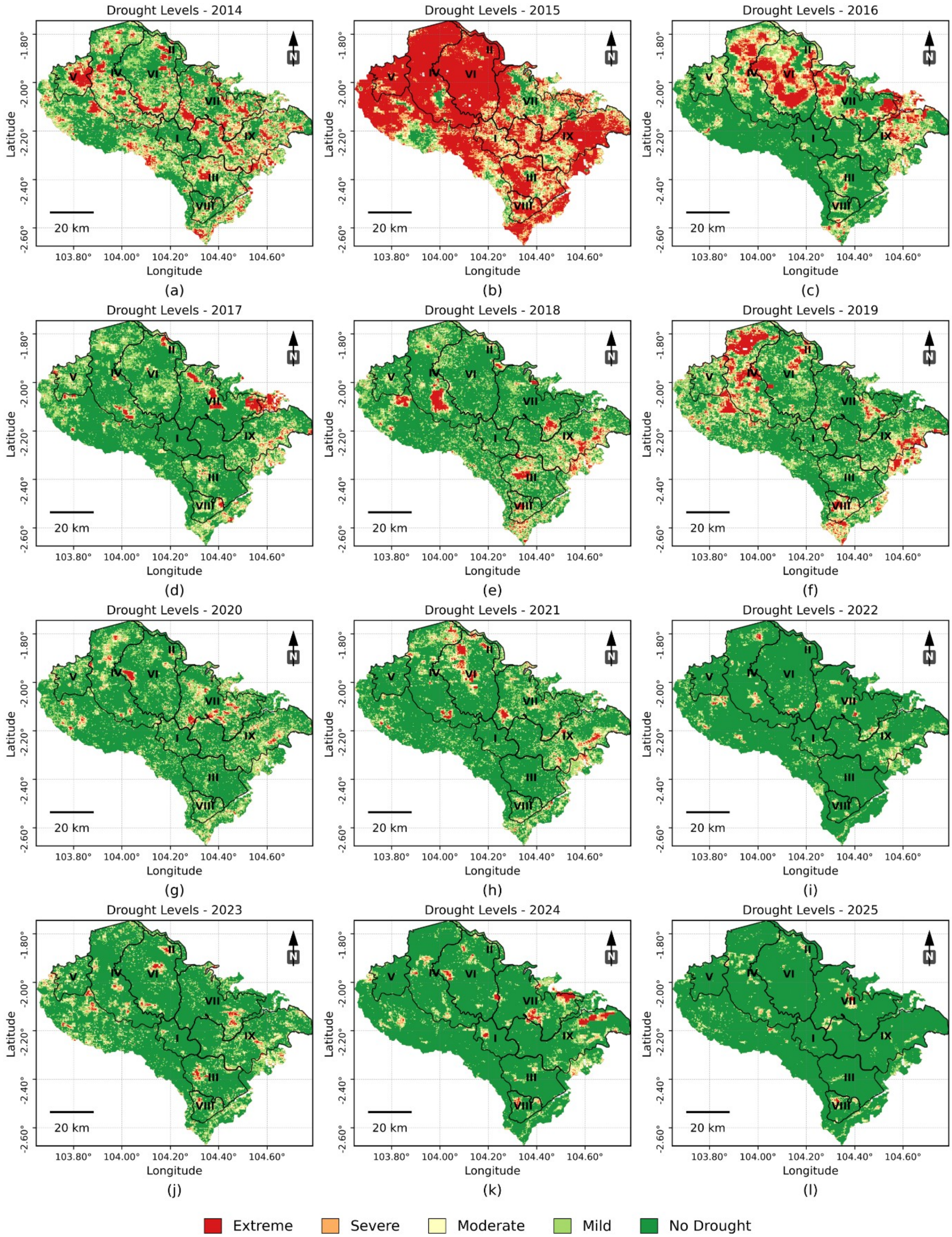

Figure 5. Spatiotemporal Distribution of Drought Severity Levels Derived from VHI Classification for Panels (a) 2014 Through (l) 2025

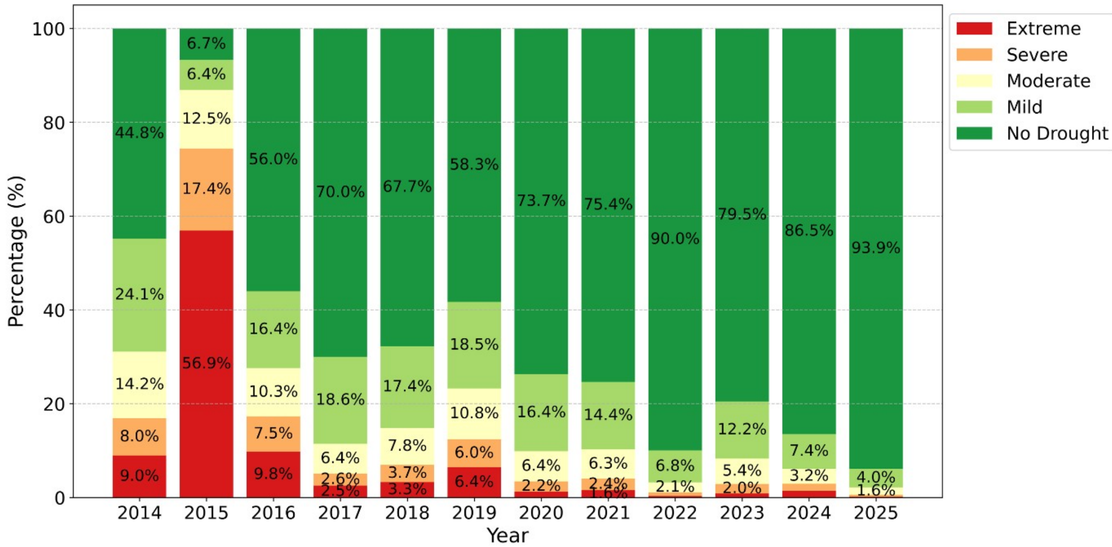

Figure 6. Annual Percentage Distribution of Drought Severity Levels from 2014 to 2025

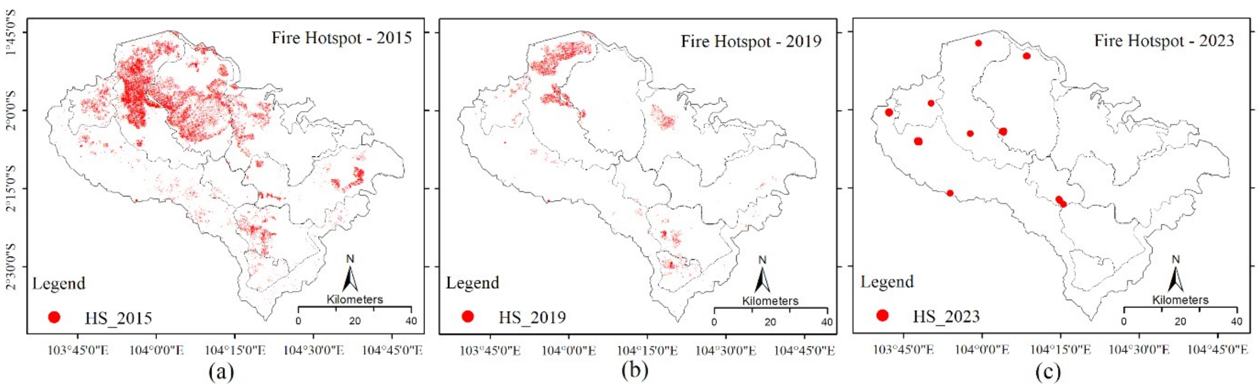

Figure 7. Spatial Distribution of VIIRS-Derived Fire Hotspots Across the Study Area for Panels (a) 2015, (b) 2019, and (c) 2023

severity. Consequently, VIIRS hotspots are best interpreted as indicators of medium-to-large, high-temperature fire activity, whereas the RBR maps provide a more spatially detailed picture of fire severity, especially for smaller burn scars. Fire-induced vegetation loss was further verified from the Landsat images, which showed lower vegetation density in the post-fire composite images (Figure 9). This implies significant peatland vegetation degradation after the fire.

3.4 Vegetation Degradation and Deforestation Dynamics

Vegetation degradation and deforestation were assessed using the NDFI derived from the SMA of the Landsat data. The index allows the detection of not only large-scale deforestation but also subtle canopy disturbances. The data reveals that the peak of deforestation transpired in 2015, succeeded by significant disruptions in 2016, 2019, 2020, and 2023 (Figure 10). The regions most severely impacted encompassed the S. Merang – S. Ngirawan watersheds, as well as the S. Lalan – S. Merang peatland management unit (Figure 11). The spatial distribution of deforestation identified from NDFI changes is consistent with MODIS land-cover transitions from forest to non-forest and with clusters of high hotspot density during major fire years (2015, 2019, 2023), supporting the reliability of the SMA-based deforestation mapping.

Apart from large-scale deforestation, partial vegetation disturbances were also observed. The disturbances primarily occurred near settlements in the western part of the study area and might be caused by selective logging, canal construction, road development, or small-scale agricultural expansion. Such disturbances gradually result in the fragmentation of forest ecosystems and the decrease in canopy density, ultimately making ecosystems more vulnerable to drought and fire. Previous studies found that the rate of groundwater level decline in disturbed peatlands was faster than in relatively undisturbed peat swamp forests due to the decrease in evapotranspiration feedback and soil water retention capacity. Therefore, vegetation degradation is likely to greatly enhance the sensitivity of peatland ecosystems to drought.

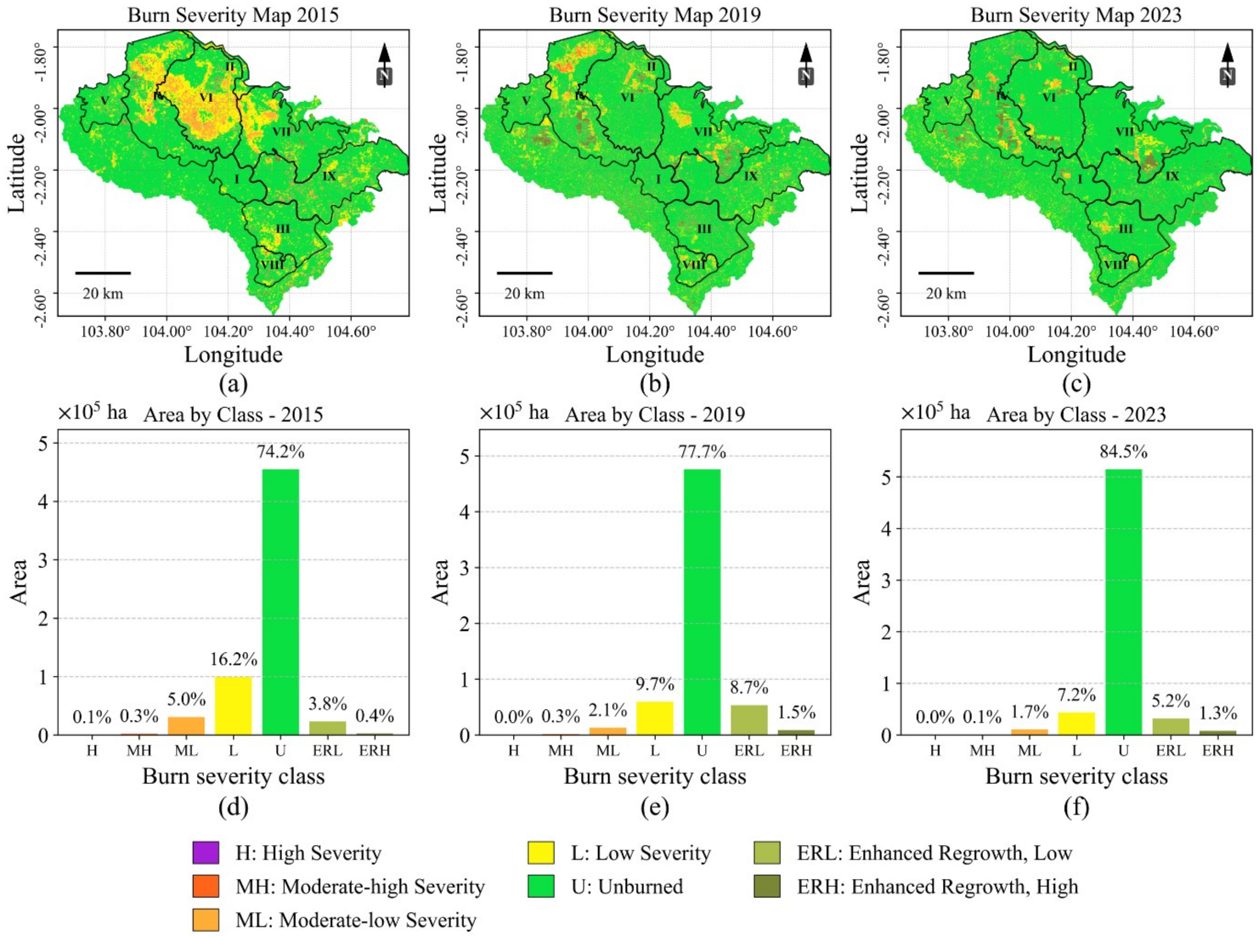

Figure 8. Burn Severity Spatial Distribution Maps for Panels (a) 2015, (b) 2019, and (c) 2023, Along with Their Corresponding Areal Statistics in Panels (d), (e), and (f)

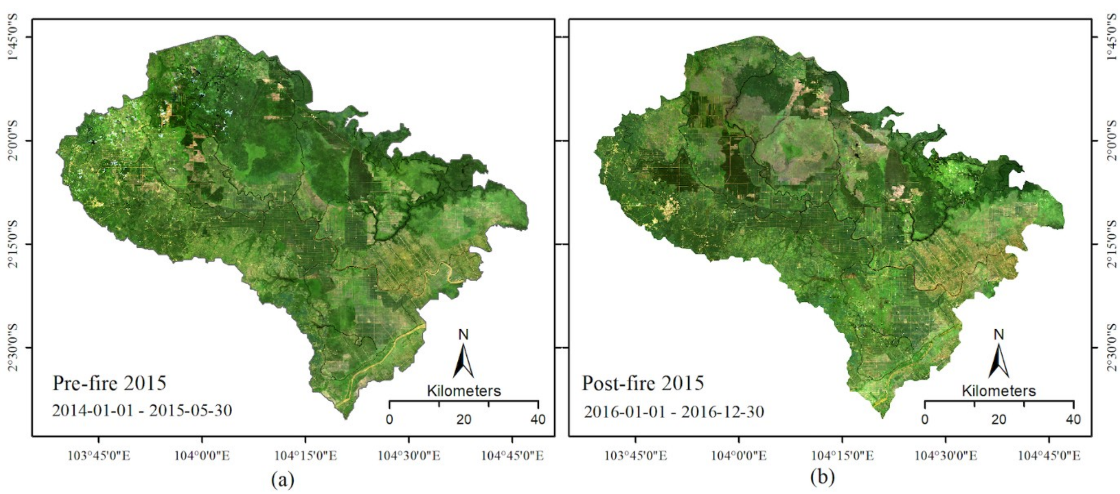

Figure 9. Landsat-8 True-Color (RGB 4-3-2) Composites Showing the Study Area Under (a) Pre-Fire And (b) Post-Fire Conditions for the 2015 Fire Event

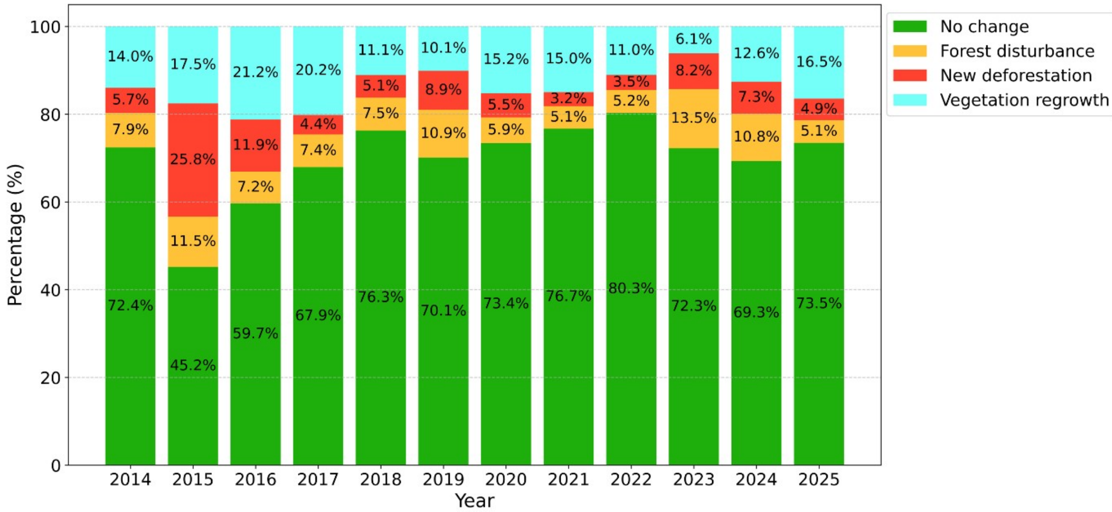

Figure 10. Annual Percentage Distribution of Forest Cover Change and Dynamics from 2014 to 2025

3.5 Hydrological Response and Surface Runoff Dynamics

The dynamics of surface runoff are highly dependent on land cover conditions. To achieve spatially explicit information on land cover, the MODIS-derived land cover data were downscaled using the SVM approach with the Landsat-derived data as the main dataset. The MODIS-derived land cover products have relatively coarse spatial resolutions (250–500 m), which may limit their use for catchment-scale hydrological modeling. With the integration of the 30 m resolution Landsat-derived data, the downscaled land cover map (Figure 12) with accuracy assessment presented in Figure 13 allows improved spatial resolution for runoff modeling (Figure 14). The accuracy evaluation of the SVM-based land cover downscaling from 2014 to 2025 shows that the classification accuracy of the SVM model is stable and reliable during the period. The confusion matrix reveals that the diagonal line contains a large concentration of accurate classification data, especially for water bodies and permanent wetlands, which also indicates good separability between classes. The overall accuracy (OA) varies from 0.64 to 0.70, with the highest accuracy in 2019, while the Kappa coefficient (κ) varies from 0.58 to 0.66, indicating a substantial level of agreement between the actual and predicted values. Some differences in accuracy between vegetation-related classes are expected in a heterogeneous landscape, but overall, the accuracy assessment shows that the SVM model is working robustly and is a reliable tool for land cover analysis over time in this region.

The results of the SCS-CN hydrological model show that there was a significant water deficit in 2015 during the El Nino period (Figure 15). The drought lasted from about May to October and the water deficit was about -116 mm. After the severe drought, hydrological conditions gradually recovered in 2016, although water availability remained limited. Surface runoff was mainly controlled by rainfall variability. However, land cover conditions also played an important role, which can be reflected from the change in the runoff coefficient from 13% in 2015 to 15% in 2016. Although there was increased rainfall in 2016, the runoff was still high due to the still low recovery of vegetation following the deforestation and degradation in 2015. These results indicate that deforestation decreases the infiltration capacity and the surface runoff ratio which is proportional to rainfall. Similar hydrological responses have been observed in several tropical catchments subjected to deforestation, which can alter the catchment water balance and influence the hydrological variability.

3.6 Spatiotemporal Impact of Deforestation on Runoff, Drought, and Fire Severity

The results of this study indicate a strong relationship between deforestation, drought severity, fire occurrence, and hydrological responses in tropical peatland ecosystems. Extensive deforestation causes the reduction of canopy density and the loss of roots that maintain the soil moisture and recharge the groundwater storage. This results in a decrease in the infiltration and an increase in surface runoff, enhancing the drying of peat during the drought. In addition, the reduction of the vegetation cover decreases the evapotranspiration and the canopy shadow which are also responsible for the maintaining of the soil moisture. Consequently, the peat layer becomes drier and the peat is more prone to fire. The spatial analysis results show that the regions with extensive deforestation correspond to the areas with severe drought and high fire severity. Fire severity analysis shows that deforested areas were frequently affected by moderate to high burn severity. The results suggest that peatland vulnerability is not only influenced by climate, but also worsened by changes in land cover.

The spatiotemporal analysis framework used in this study is useful in identifying cascading effects among climate drivers, land cover changes, hydrological responses and ecosystem disturbances.

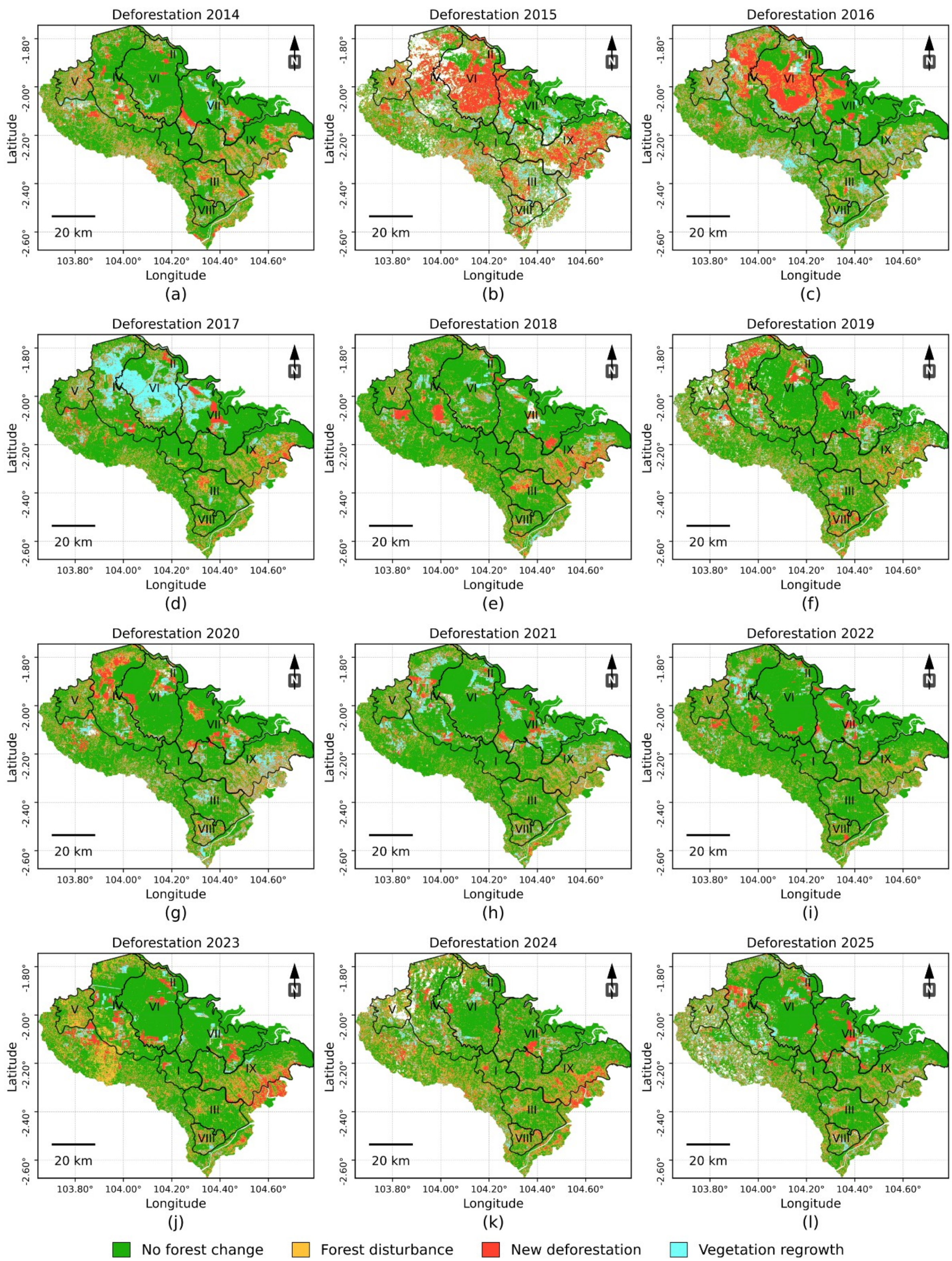

Figure 11. Annual Spatial Maps of Forest Disturbance, Deforestation, and Vegetation Regrowth from 2014 to 2025, Designated Chronologically from Panels (a) to (l)

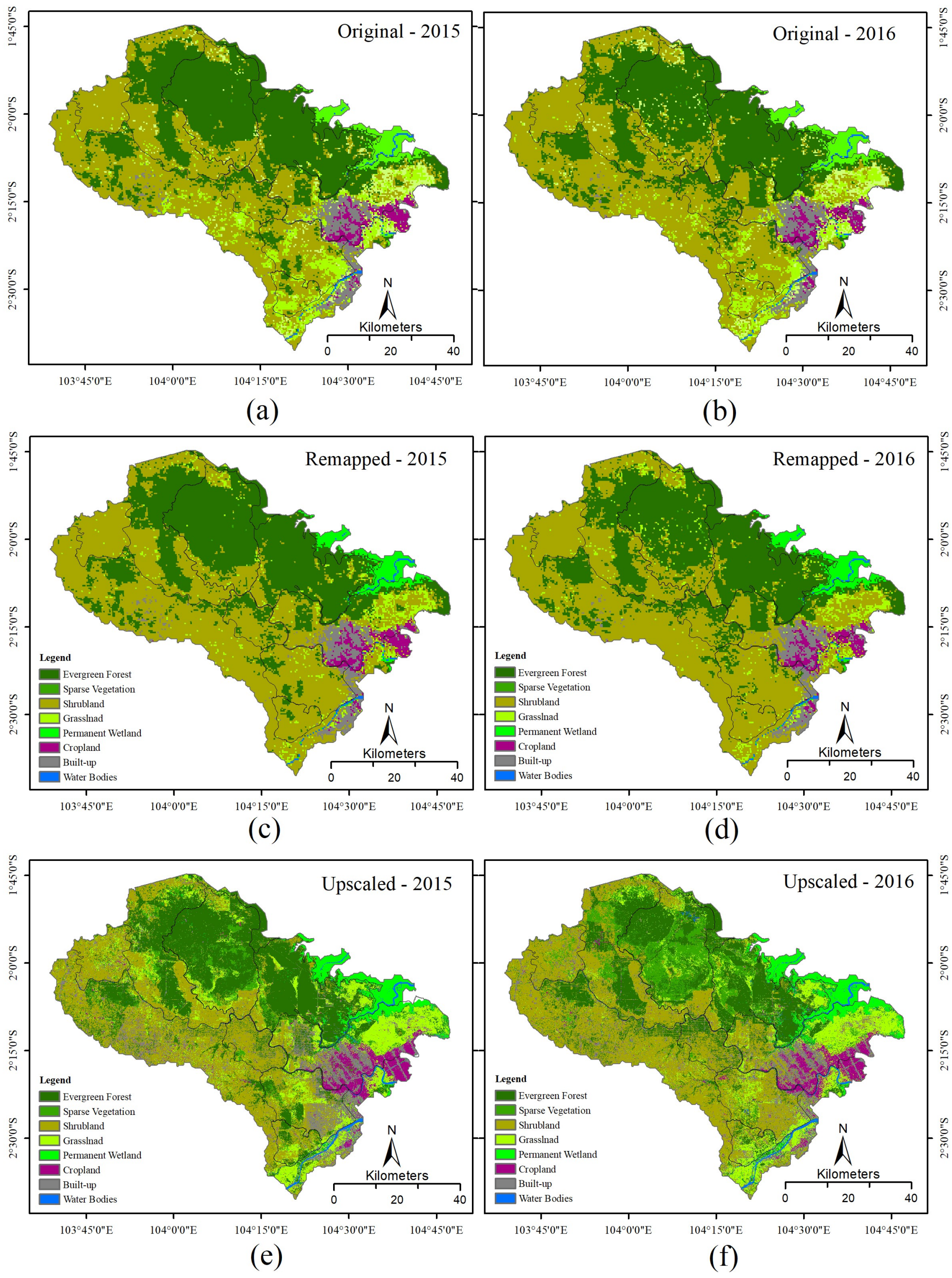

Figure 12. Land Cover Maps for 2015 and 2016 Showing Original MODIS Data in Panels (a-b), Remapped Results in Panels (c–d), and Landsat-8 Upscaled Results in Panels (e–f)

3.7 Relationships Analysis Among Deforestation, Runoff, Drought, and Fire Severity

The correlations revealed different values of linkages of fire severity and deforestation, and drought and runoff (Figure 16), implying partial decoupling of the environment. There existed a strong negative correlation between fire severity and deforestation ($r = -0.731$). It implies that there exists an inverse relation between fire severity and deforestation, meaning that high values of fire severity would have low dNDFI. In other words, pixels with high fire severity are less likely to be affected by deforestation.

The association between deforestation and drought was

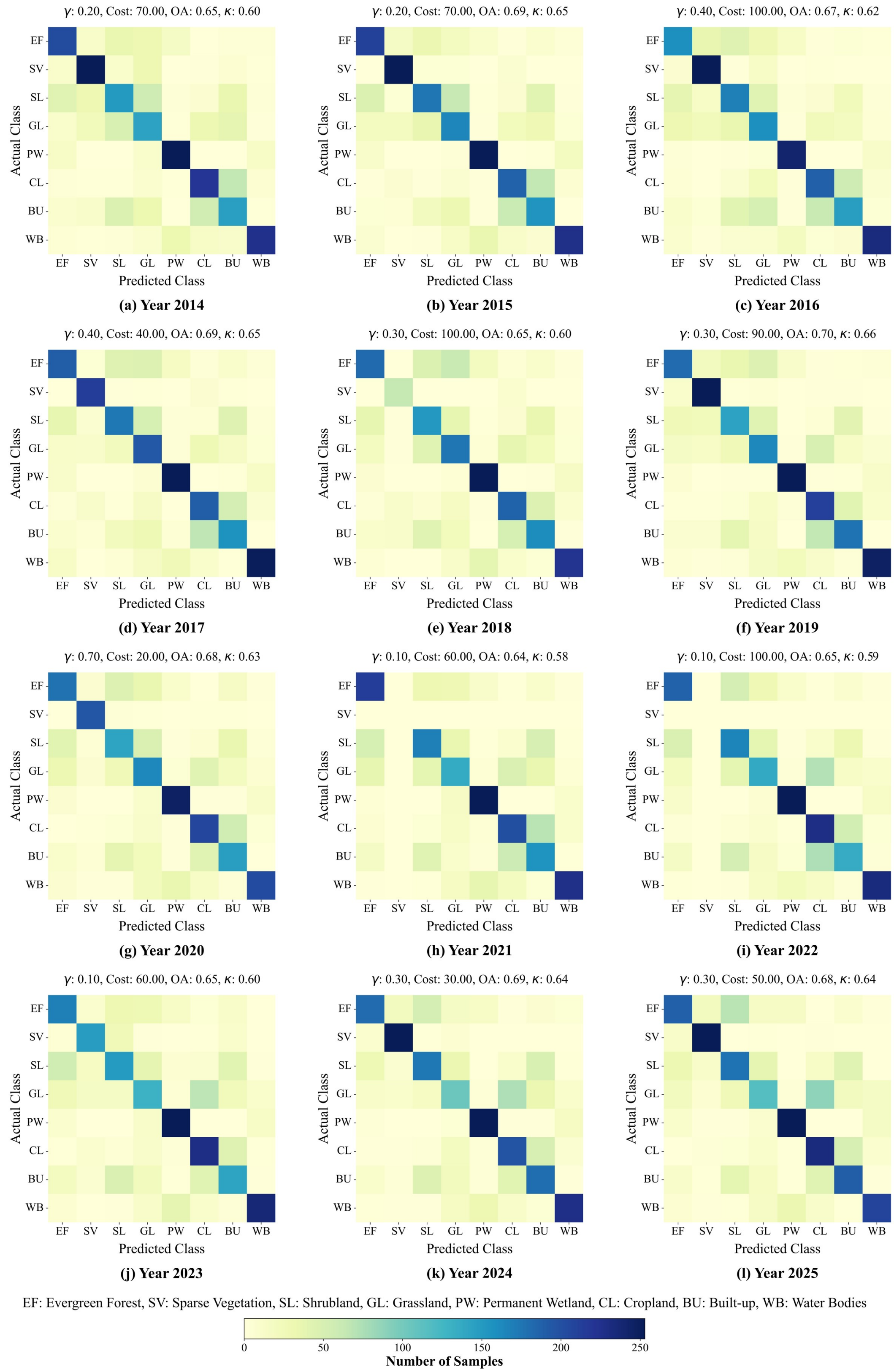

Figure 13. Confusion Matrices, Optimum Parameters (γ and Cost), Overall Accuracy, and Kappa for SVM-Based Land Cover Downscaling from 2014 to 2025, Chronologically Designated Across Panels (a) Through (l)

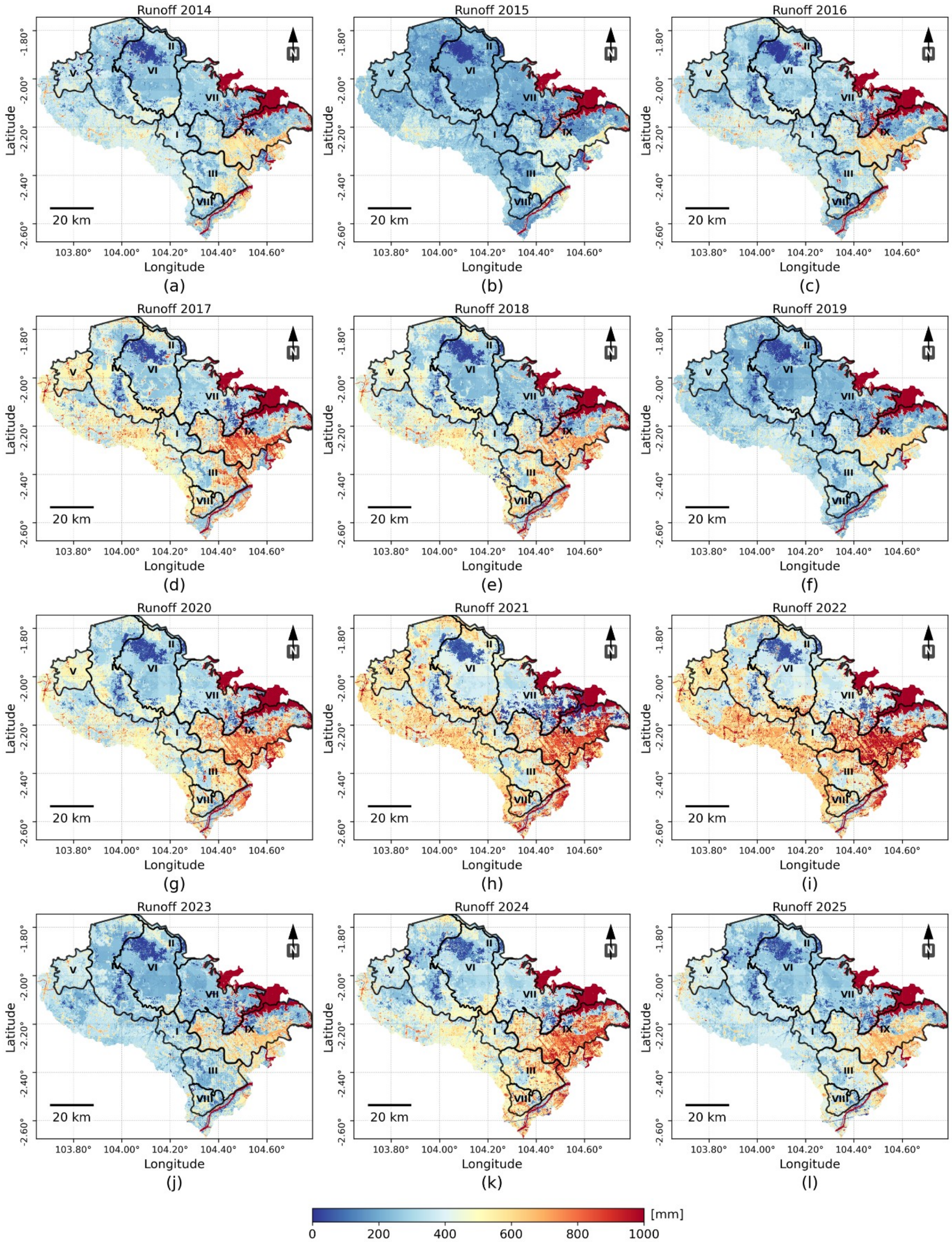

Figure 14. Spatiotemporal Distribution of Annual Surface Runoff Across the Study Area for Panels (a) 2014 Through (l) 2025

moderately positive ($r = 0.423$) meanwhile, indicating that areas with higher vegetation health stresses and drought (represented by VHI) had higher rates of deforestation. This suggests that the biophysical effects of vegetation in supporting soil moisture in the peatland ecosystem could also contribute to the association between deforestation and drought. The relationship between fire severity and drought was weakly negative ($r = -0.237$); in other words, drought does not have a controlling effect on fire. These results indicate that factors other than drought may control fire in the study area.

Drought–runoff ($r = -0.067$), deforestation–runoff ($r = -0.095$), and fire severity–runoff ($r = 0.027$) had very low

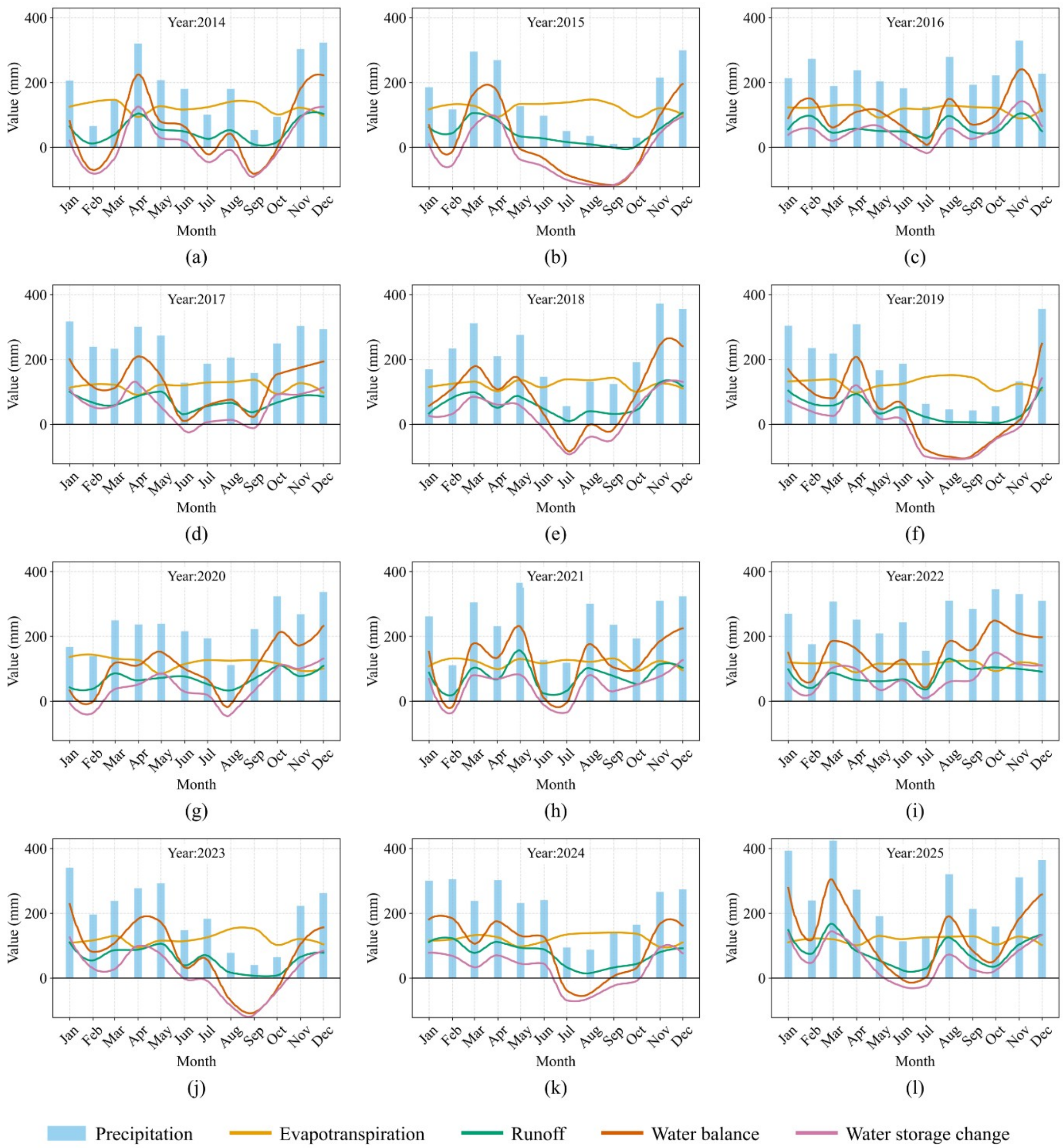

Figure 15. Monthly Variations of Precipitation, Evapotranspiration, Runoff, Water Balance, and Water Storage Change Across the Study Area for Panels (a) 2014 Through (l) 2025

values and suggest that factors other than disturbance could control runoff. Therefore, it appears that runoff may depend more on other factors than deforestation and fire severity, such as precipitation, soil, and peat storage capacity.

From the above results, it can be concluded that although deforestation is important for intensifying drought, its effect on runoff together with fire severity is minimal, implying a decoupled relationship between disturbance variables and runoff. Possible explanations for this decoupling include climatic conditions, such as water availability (e.g., the role of precipitation or recharge in groundwater) and the effects of subsurface waters.

3.8 Uncertainty Analysis and Error Propagation

Uncertainty in this study arises from many datasets (Landsat, MODIS, CHIRPS, GLDAS) and disseminates throughout the analytical framework. Landsat surface reflectance has errors of ±5–10% due to atmospheric adjustment and cloud masking. This affects the NDFI fractions derived from SMA in mixed pixels (Roy et al., 2014; Vermote et al., 2016). MODIS land cover has 70–80% accuracy (±20–30% pixel level error) globally. This impacts Curve Number (CN) estimation. Tropical CHIRPS rainfall bias is ±10–20%, and soil moisture/temperature uncertainties from GLDAS are ±10–20% in comparison to in-situ data (Friedl et al., 2010; Funk et al., 2015; Rodell et al., 2004).

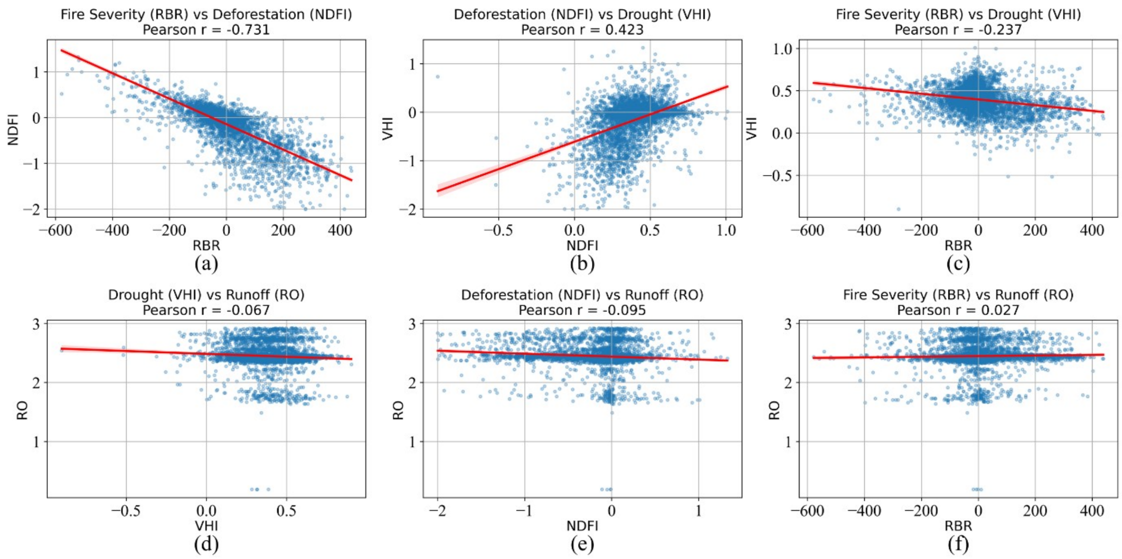

Figure 16. Scatter Plots and Linear Regressions Describing Pairwise Relationships Between Standardized Indices of Fire Severity (RBR), Deforestation (DNDFI), Drought (VHI), and Runoff (RO) Across the Study Area

Sensitivity analysis measured propagation: a 10% change in rainfall leads to a 10.5–18% change in runoff because SCS-CN is not linear; a 5 CN unit change leads to a 1–15% change in runoff; and a 0.05 VHI threshold change moves the extreme drought area by less than 5%. These are in line with model behavior, where rainfall and CN are the main sources of uncertainty while drought classification is strong. The combination of independent datasets reduces systematic bias, which is supported by the fact that CHIRPS rainfall anomalies, GLDAS soil moisture, MODIS vegetation and VIIRS fire patterns all show the same trends. This confirms the main conclusions despite the existence of some individual uncertainties.

3.9 Comparison with Previous Studies

To place our findings in the context of existing literature, we compared the main methodological characteristics and key results of this study with several representative studies that focus on SMA-based deforestation mapping, VHI-based drought monitoring, RBR-based fire severity assessment, and SCS-CN runoff modelling (Table 2). The comparison highlights substantial differences in terms of ecosystem type, temporal coverage, and the number of processes analysed jointly. Most previous works target a single component or a limited combination of indicators and are often conducted in non-peatland forests or at broader regional scales.

In contrast, our framework simultaneously integrates SMA-derived NDFI, SCS-CN-based runoff coefficients, VHI-based drought categories, and RBR-based fire severity classes over a 12-year period (2014–2025) for nine peat hydrological units in South Sumatra. This joint analysis enables a spatially explicit assessment of how deforestation and vegetation degradation modify hydrological response, drought conditions, and fire severity in a fire-prone tropical peatland landscape—an aspect that is rarely addressed in earlier studies, which typically examine these processes separately.

As summarized in Table 2, previous studies have made important contributions to understanding individual components such as deforestation, drought, or fire severity, but they usually analyse these processes in isolation or in non-peatland contexts. By jointly integrating SMA-based NDFI, SCS-CN runoff, VHI, and RBR over a multi-year period in tropical peat hydrological units, our study extends this body of work by explicitly quantifying the linkages between vegetation degradation, hydrological response, drought intensity, and fire severity. This integrated perspective is particularly relevant for designing data-driven strategies for peatland fire mitigation and hydrological management in South Sumatra and similar regions. These results also corroborate recent studies at the regional scale that linked rainfall variability and drought anomalies to forest and land fire dynamics in Sumatra (Akhsan et al., 2023; Suhadi et al., 2023). In comparison with those studies, the present work extends the regional evidence by integrating deforestation, runoff, drought severity, and fire severity within a single spatiotemporal framework focused on tropical peat hydrological units.

The integrated patterns of deforestation, runoff, drought, and fire severity revealed in this study also provide practical guidance for peatland management. In particular, peat hydrological units that have experienced recurrent extreme drought, high fire severity, and extensive vegetation degradation should be prioritised for interventions that limit further forest loss, restore vegetated cover, and stabilise groundwater levels through canal blocking, rewetting, and improved water-table management. By using the spatially explicit indicators developed here (NDFI-based deforestation, SCS-CN runoff coefficients, VHI drought classes, and RBR fire severity), managers can identify high-risk sub-catchments, align restoration efforts with areas of greatest vulnerability, and monitor the effectiveness of existing peatland policies aimed at reducing fire risk and maintaining hydrological stability in South Sumatra's peat hydrological units.

4. CONCLUSION

This study demonstrates that a complex interplay existed among climate variation, deforestation, hydrological process, and fire dynamics in tropical peatland ecosystem of South Sumatra. An extreme drought event, which occurred particularly in 2015, 2019, and 2023, significantly reduced the soil moisture and the peat water table, which would eventually increase the vegetation stress and fire risk. The year 2015 is the most critical year, where severe drought, high level of vegetation degradation, and massive peatland fires occurred simultaneously. Deforestation exacerbated the climate-driven impacts by decreasing the infiltration and weakening the ecosystem's capacity to store the water. Such changes resulted in an increase in surface runoff and accelerating peat drying, which eventually increased the fire severity. The integration of SMA, NDFI-based deforestation detection, VHI-based drought monitoring, RBR-based fire severity analysis, and SCS-CN-based hydrological analysis provides a useful framework to investigate the cascading effect among climate variation, land cover change, and ecosystem response. Therefore, maintaining the vegetation cover and preventing further deforestation are the essential practices to maintain a stable hydrological condition of the peatland and reduce the fire risk. Rewetting and revegetation of peatland could significantly reduce the drought vulnerability and mitigate the massive peat fires in Indonesia.

5. ACKNOWLEDGMENT

We thank the Directorate of Research and Community Service, Directorate General of Research and Development, Ministry of Higher Education, Science, and Technology, for the support provided through the State University Operational Assistance Program, under the Research Program Contract No. 109/C3/DT.0500/PL/2025.

REFERENCES

Akhsan, H., M. Irfan, S. Supari, and I. Iskandar (2023). Dynamics of Extreme Rainfall and Its Impact on Forest and Land Fires in the Eastern Coast of Sumatra. *Science and Technology Indonesia*, **8**(3); 403–413

Almouctar, M. A. S., Y. Wu, F. Zhao, and C. Qin (2024). Drought Analysis Using Normalized Difference Vegetation Index and Land Surface Temperature Over Niamey Region, the Southwestern of the Niger Between 2013 and 2019. *Journal of Hydrology: Regional Studies*, **52**; 101689

Brandão, A. R. A., D. Schwamback, A. S. Ballarin, J. J. Ramirez-Avila, J. G. Vasconcelos Neto, and P. T. S. Oliveira (2025). Toward a Better Understanding of Curve Number and Initial Abstraction Ratio Values from a Large Sample of Watersheds Perspective. *Journal of Hydrology*, **655**; 132941

Bruijnzeel, L. A. (2004). Hydrological Functions of Tropical Forests: Not Seeing the Soil for the Trees? *Agriculture, Ecosystems & Environment*, **104**(1); 185–228

Bullock, E. L., C. E. Woodcock, C. Souza, and P. Olofsson (2020). Satellite-Based Estimates Reveal Widespread Forest Degradation in the Amazon. *Global Change Biology*, **26**(5); 2956–2969

Burka, A., B. Biazin, and W. Bewket (2024). Spatial Drought Occurrences and Distribution Using VCI, TCI, VHI, and Google Earth Engine in Bilate River Watershed, Rift Valley of Ethiopia. *Geomatics, Natural Hazards and Risk*, **15**(1); 2377672

Cortes, C. and V. Vapnik (1995). Support-Vector Networks. *Machine Learning*, **20**(3); 273–297

Datta, A. and R. Krishnamoorti (2022). Understanding the Greenhouse Gas Impact of Deforestation Fires in Indonesia and Brazil in 2019 and 2020. *Frontiers in Climate*, **4**; 799632

Field, R. D., G. R. van der Werf, and S. S. P. Shen (2009). Human Amplification of Drought-Induced Biomass Burning in Indonesia Since 1960. *Nature Geoscience*, **2**(3); 185–188

Friedl, M. A., D. Sulla-Menashe, B. Tan, A. Schneider, N. Ramankutty, A. Sibley, and X. Huang (2010). MODIS Collection 5 Global Land Cover: Algorithm Refinements and Characterization of New Datasets. *Remote Sensing of Environment*, **114**(1); 168–182

Funk, C., P. Peterson, M. Landsfeld, D. Pedreros, J. Verdin, S. Shukla, G. Husak, J. Rowland, L. Harrison, A. Hoell, and J. Michaelsen (2015). The Climate Hazards Infrared Precipitation With Stations—A New Environmental Record for Monitoring Extremes. *Scientific Data*, **2**; 150066

Halbgewachs, M., M. Wegmann, and E. da Ponte (2022). A Spectral Mixture Analysis and Landscape Metrics Based Framework for Monitoring Spatiotemporal Forest Cover Changes: A Case Study in Mato Grosso, Brazil. *Remote Sensing*, **14**(8); 1907

Hasan, A. F., F. Laurent, F. Messner, C. Bourgoin, and L. Blanc (2019). Cumulative Disturbances to Assess Forest Degradation Using Spectral Unmixing in the Northeastern Amazon. *Applied Vegetation Science*, **22**(3); 394–408

Hengl, T. (2018). Soil Texture Classes (USDA System) for 6 Soil Depths (0, 10, 30, 60, 100 and 200 cm) at 250 m (v0.2) [Data Set]

Hou, Y., X. Wei, M. Zhang, I. F. Creed, S. G. McNulty, and S. F. B. Ferraz (2023). A Global Synthesis of Hydrological Sensitivities to Deforestation and Forestation. *Forest Ecology and Management*, **529**; 120718

Huijnen, V., M. J. Wooster, J. W. Kaiser, D. L. A. Gaveau, J. Flemming, M. Parrington, A. Inness, D. Murdiyarso, B. Main, and M. van Weele (2016). Fire Carbon Emissions Over Maritime Southeast Asia in 2015 Largest Since 1997. *Scientific Reports*, **6**; 26886

Kettridge, N., M. R. Turetsky, J. H. Sherwood, D. K. Thompson, C. A. Miller, B. W. Benscoter, M. D. Flannigan, B. M. Wotton, and J. M. Waddington (2015). Moderate Drop in Water Table Increases Peatland Vulnerability to Post-Fire

Regime Shift. *Scientific Reports*, **5**; 8063

Kiely, L., D. V. Spracklen, S. R. Arnold, E. Papargyropoulou, L. Conibear, C. Wiedinmyer, C. Knote, and H. A. Adrianto (2021). Assessing Costs of Indonesian Fires and the Benefits of Restoring Peatland. *Nature Communications*, **12**; 7044

Ma, S., S. Zhou, B. Yu, and J. Song (2024). Deforestation-Induced Runoff Changes Dominated by Forest-Climate Feedbacks. *Science Advances*, **10**(11)

Mandailing, P. M., W. Mardiansyah, M. Irfan, A. Arsali, and I. Iskandar (2020). Characteristics of Diurnal Rainfall Over Peatland Area of South Sumatra, Indonesia. *Science and Technology Indonesia*, **5**(4); 136–141

Michel, C., V. Andréassian, and C. Perrin (2005). Soil Conservation Service Curve Number Method: How to Mend a Wrong Soil Moisture Accounting Procedure? *Water Resources Research*, **41**(2)

Miller, J. D. and A. E. Thode (2007). Quantifying Burn Severity in a Heterogeneous Landscape With a Relative Version of the Delta Normalized Burn Ratio (dNBR). *Remote Sensing of Environment*, **109**(1); 66–80

Mishra, S., S. E. Page, A. R. Cobb, J. S. H. Lee, A. J. Jovani-Sancho, S. Sjögersten, A. Jaya, Aswandi, and D. A. Wardle (2021). Degradation of Southeast Asian Tropical Peatlands and Integrated Strategies for Their Better Management and Restoration. *Journal of Applied Ecology*, **58**(7); 1370–1387

Mishra, S. K. and V. P. Singh (2003). SCS-CN Method. In *Soil Conservation Service Curve Number (SCS-CN) Methodology*. Springer, Dordrecht, pages 84–146

Mockus, V. (1949). Estimation of Total (Peak Rates of) Surface Runoff for Individual Storms. Technical report, Washington, DC

Morresi, D., R. Marzano, E. Lingua, R. Motta, and M. Garbarino (2022). Mapping Burn Severity in the Western Italian Alps Through Phenologically Coherent Reflectance Composites Derived From Sentinel-2 Imagery. *Remote Sensing of Environment*, **269**; 112800

Nikonovas, T., A. Spessa, S. H. Doerr, G. D. Clay, and S. Mezbahuddin (2020). Near-Complete Loss of Fire-Resistant Primary Tropical Forest Cover in Sumatra and Kalimantan. *Communications Earth & Environment*, **1**; 65

Page, S. E., F. Siegert, J. O. Rieley, H. V. D. V. Boehm, A. Jaya, and S. Limin (2002). The Amount of Carbon Released From Peat and Forest Fires in Indonesia During 1997. *Nature*, **420**(6911); 61–65

Parks, S., G. Dillon, and C. Miller (2014). A New Metric for Quantifying Burn Severity: The Relativized Burn Ratio. *Remote Sensing*, **6**(3); 1827–1844

Pertiwi, N., T. W. Tsusaka, N. Sasaki, and E. Gunawan (2021). Peatland Conservation Strategies and Carbon Pricing Possibilities for Climate Change Mitigation in Indonesia: A Review. *IOP Conference Series: Earth and Environmental Science*, **892**(1); 012061

Pesaresi, M., M. Schiavina, P. Politis, S. Freire, K. Krasnodębska, J. H. Uhl, A. Carioli, C. Corbane, L. Dijkstra, P. Florio, H. K. Friedrich, J. Gao, S. Leyk, L. Lu, L. Maffenini, I. Mari-Rivero, M. Melchiorri, V. Syrris, J. Van Den Hoek, and T. Kemper (2024). Advances on the Global Human Settlement Layer by Joint Assessment of Earth Observation and Population Survey Data. *International Journal of Digital Earth*, **17**(1); 2390454

Peña-Arancibia, J. L., L. A. Bruijnzeel, M. Mulligan, and A. I. van Dijk (2019). Forests as 'Sponges' and 'Pumps': Assessing the Impact of Deforestation on Dry-Season Flows Across the Tropics. *Journal of Hydrology*, **574**; 946–963

Pisner, D. A. and D. M. Schnyer (2020). Support Vector Machine. In *Machine Learning*. Elsevier, pages 101–121

Potić, I., L. M. Mihajlović, V. Šimunić, N. B. Ćurčić, and M. Milinčić (2022). Deforestation as a Cause of Increased Surface Runoff in the Catchment: Remote Sensing and SWAT Approach—A Case Study of Southern Serbia. *Frontiers in Environmental Science*, **10**; 896404

Rodell, M., P. R. Houser, U. Jambor, J. Gottschalck, K. Mitchell, C.-J. Meng, K. Arsenault, B. Cosgrove, J. Radakovich, M. Bosilovich, J. K. Entin, J. P. Walker, D. Lohmann, and D. Toll (2004). The Global Land Data Assimilation System. *Bulletin of the American Meteorological Society*, **85**(3); 381–394

Roy, D. P., M. A. Wulder, T. R. Loveland, C. E. Woodcock, R. G. Allen, M. C. Anderson, D. Helder, J. R. Irons, D. M. Johnson, R. Kennedy, T. A. Scambos, C. B. Schaaf, J. R. Schott, Y. Sheng, E. F. Vermote, A. S. Belward, R. Bindschadler, W. B. Cohen, F. Gao, J. D. Hipple, P. Hostert, J. Huntington, C. O. Justice, A. Kilic, V. Kovalskyy, Z. P. Lee, L. Lymburner, J. G. Masek, J. McCorkel, Y. Shuai, R. Trezza, J. Vogelmann, R. H. Wynne, and Z. Zhu (2014). Landsat-8: Science and Product Vision for Terrestrial Global Change Research. *Remote Sensing of Environment*, **145**; 154–172

Singh, H., M. A. Alam, P. J. Sharma, and K. S. Rautela (2023). A Comparison of the SCS-CN-Based Models for Hydrological Simulation of the Aghanashini River, Karnataka, India. *AQUA — Water Infrastructure, Ecosystems and Society*, **72**(4); 507–519

Soil Conservation Service (1972). *National Engineering Handbook, Section 4: Hydrology*. U.S. Department of Agriculture, Washington, DC

Souza, C. M., D. A. Roberts, and M. A. Cochrane (2005). Combining Spectral and Spatial Information to Map Canopy Damage from Selective Logging and Forest Fires. *Remote Sensing of Environment*, **98**(2–3); 329–343

Souza, J. C., J. V. Siqueira, M. H. Sales, A. V. Fonseca, J. G. Ribeiro, I. Numata, M. A. Cochrane, C. P. Barber, D. A. Roberts, and J. Barlow (2013). Ten-Year Landsat Classification of Deforestation and Forest Degradation in the Brazilian Amazon. *Remote Sensing*, **5**(11); 5493–5513

Soverel, N. O., D. D. B. Perrakis, and N. C. Coops (2010). Estimating Burn Severity from Landsat dNBR and RdNBR Indices Across Western Canada. *Remote Sensing of Environment*, **114**(9); 1896–1909

Suhadi, S., I. Iskandar, S. Supari, M. Irfan, and H. Akhsan

(2023). Extreme Drought Assessment in Sumatra-Indonesia Using SPI and EDI. *Science and Technology Indonesia*, **8**(4); 691–700

Szumińska, D., S. Czapiewski, and P. Sewerniak (2023). Natural and Anthropogenic Factors Influencing Changes in Peatland Management in Poland. *Regional Environmental Change*, **23**(1); 5

Turetsky, M. R., B. Benscoter, S. Page, G. Rein, G. R. Van Der Werf, and A. Watts (2015). Global Vulnerability of Peatlands to Fire and Carbon Loss. *Nature Geoscience*, **8**(1); 11–14

United States Department of Agriculture, N.R.C.S. (2004). *National Engineering Handbook, Part 630: Hydrology*. U.S. Department of Agriculture, Washington, DC

Vermote, E., C. Justice, M. Claverie, and B. Franch (2016). Preliminary Analysis of the Performance of the Landsat 8/OLI Land Surface Reflectance Product. *Remote Sensing of Environment*, **185**; 46–56

Whitman, E., M. Parisien, D. K. Thompson, R. J. Hall, R. S. Skakun, and M. D. Flannigan (2018). Variability and Drivers of Burn Severity in the Northwestern Canadian Boreal Forest. *Ecosphere*, **9**(2); e02128

Yule, C. M. (2010). Loss of Biodiversity and Ecosystem Functioning in Indo-Malayan Peat Swamp Forests. *Biodiversity and Conservation*, **19**(2); 393–409

Zeng, J., R. Zhang, Y. Qu, V. A. Bento, T. Zhou, Y. Lin, X. Wu, J. Qi, W. Shui, and Q. Wang (2022). Improving the Drought Monitoring Capability of VHI at the Global Scale via Ensemble Indices for Various Vegetation Types from 2001 to 2018. *Weather and Climate Extremes*, **35**; 100412

Zeng, J., T. Zhou, Y. Qu, V. A. Bento, J. Qi, Y. Xu, Y. Li, and Q. Wang (2023). An Improved Global Vegetation Health Index Dataset in Detecting Vegetation Drought. *Scientific Data*, **10**(1); 338

